

## UPDATED RADIO $\Sigma - D$ RELATION FOR GALACTIC SUPERNOVA REMNANTS

M. Z. Pavlović<sup>1</sup>, A. Dobardžić<sup>1</sup>, B. Vukotić<sup>2</sup> and D. Urošević<sup>1</sup>

<sup>1</sup>*Department of Astronomy, Faculty of Mathematics, University of Belgrade  
Studentski trg 16, 11000 Belgrade, Serbia*

E-mail: marko@math.rs, aleksandra@math.rs, dejanu@math.rs

<sup>2</sup>*Astronomical Observatory, Volgina 7, 11060 Belgrade 38, Serbia*

E-mail: bvukotic@aob.rs

(Received: October 23, 2014; Accepted: November 13, 2014)

**SUMMARY:** We present the updated empirical radio surface-brightness-to-diameter ( $\Sigma - D$ ) relation for supernova remnants (SNRs) in our Galaxy. Our original calibration sample of Galactic SNRs with independently determined distances (Pavlović et al. 2013, hereafter Paper I) is reconsidered and updated with data which became available in the past two years. The orthogonal fitting procedure and probability-density-function-based (PDF) method are applied to the calibration sample in the  $\log \Sigma - \log D$  plane. Non-standard orthogonal regression keeps the  $\Sigma - D$  and  $D - \Sigma$  relations invariant within estimated uncertainties. Our previous Monte Carlo simulations verified that the slopes of the empirical  $\Sigma - D$  relation should be determined by using the orthogonal regression, because of its good performances for data sets with severe scatter. The updated calibration sample contains 65 shell SNRs. 6 new Galactic SNRs are added to the sample from Paper I, one is omitted and distances are changed for 10 SNRs. The slope derived is here slightly steeper ( $\beta \approx 5.2$ ) than the  $\Sigma - D$  slope in Paper I ( $\beta \approx 4.8$ ). The PDF method relies on data points density maps which can provide more reliable calibrations that preserve more information contained in the calibration sample. We estimate distances to five new faint Galactic SNRs discovered for the first time by Canadian Galactic Plane Survey, and obtained distances of 2.3, 4.0, 1.3, 2.9 and 4.7 kiloparsecs for G108.5+11.0, G128.5+2.6, G149.5+3.2, G150.8+3.8 and G160.1–1.1, respectively. The updated empirical relation is used to estimate distances of 160 shell Galactic SNRs and new results change their distance scales up to 15 per cent, compared to the results from Paper I. The PDF calculation can provide even few times higher or lower values in comparison with the orthogonal fit, as it uses a totally different approach. However, on average, this difference is 32, 24 and 18 per cent for mode, median and mean distances.

**Key words.** ISM: supernova remnants – methods: statistical – radio continuum: ISM

### 1. INTRODUCTION

The reliable distance determination to Galactic supernova remnants (SNRs) is necessary for obtaining their basic parameters, such as size, age and

explosion energy. It also helps us to study their evolution and to describe the production of cosmic rays (CRs). There are several methods for determination distances to Galactic SNRs such as: from historical records of supernovae (SNe), from proper mo-

tions and radial velocities, kinematic observations, coincidences with HI, HII and molecular clouds, OB associations and pulsars, HI absorption and polarization, optical extinction, low frequency radio absorption, CO emission and from X-ray observations (Green 1984, Zhu and Tian 2014).

However, when distance determination by the above mentioned methods is not possible, the distance of a Galactic SNR is commonly estimated by using the radio surface brightness - diameter relation ( $\Sigma - D$ ). The relation connecting the radio surface brightness at frequency  $\nu$  and diameter of SNR is given as:

$$\Sigma_\nu(D) = AD^{-\beta}, \quad (1)$$

where  $A$  is thought to depend on properties of the SN explosion such as the SN explosion energy, the mass of the ejected matter and also on the properties of ISM such as density of the ISM, magnetic field strength, etc, while the parameter  $\beta$  is thought to be independent of these properties (Arbutina and Urošević 2005). The slope  $\beta$  explicitly depends on the spectral index  $\alpha$  of the integrated radio emission from the remnant (defined in the sense,  $S_\nu \propto \nu^{-\alpha}$ , where  $S_\nu$  is the flux density at frequency  $\nu$ ), as follows from theoretical work (first derived for SNRs; Shklovskii 1960). This relation is applicable to shell-type SNRs but it can also be used for composite remnants if we separate the surrounding shell flux and flux originating from the central regions (Case and Bhattacharya 1998).

Despite of all the criticism of the  $\Sigma - D$  relation (see for example Green 1984, 2004), it remains an important tool in estimating distances to SNRs in cases where other methods are not applicable.

Calibration is done by linearizing the above Eq. (1) and applying some of the standard fitting techniques. Parameters  $A$  and  $\beta$  are then obtained by fitting the data for a sample of SNRs of known distances (usually called calibrators). After the calibration, the relation can be used to determine the

distance to a particular SNR by measuring its flux density and angular diameter. In our previous paper (Pavlović *et al.* 2013, hereafter Paper I), we showed that applying some non-standard fitting procedures, instead of (standard) the vertical regression, can result in different parameters of the  $\Sigma - D$  relation for shell SNRs. We also emphasized a very important consequence of our analysis: orthogonal offsets are more reliable and stable over other types of offsets.

Following our approach from Paper I, we present here an updated empirical radio  $\Sigma - D$  relation for Galactic SNRs. The new relation is now based on the extended and updated calibration sample, containing 65 Galactic SNRs: 6 new SNRs were added, one is omitted from the previous calibration sample and the distance was changed for 10 remnants in accordance with the new observations.

## 2. ANALYSIS AND RESULTS

### 2.1. The updated calibration sample and corresponding $\Sigma - D$ relation

The updated Galactic sample of 65 shell Galactic SNRs with direct distance estimates, which is used to derive the new  $\Sigma - D$  relation, is in Table 1. The frequency of 1 GHz for surface brightness  $\Sigma$  is chosen because flux density measurements at frequencies, presented, both above and below this value are usually available. Usually, the flux density at 1 GHz is not a measured value, but is derived from the observed radio spectrum of the SNR, following the dependence  $S_\nu \propto \nu^{-\alpha}$ .

Similar to Paper I, our Galactic sample also includes five composite SNRs for which it was possible to separate the shell flux density from the pulsar wind nebula (PWN) flux density or they simply have a pure shell structure in radio domain. These SNRs are: G11.2-0.3, G93.3+6.9 (DA 530), G189.1+3.0 (IC 443), G338.3-0.0 and G344.7-0.1.

**Table 1:** Shell SNRs with known distances<sup>a</sup> - the calibration sample consists of 65 SNRs.

No.	Catalog name	Other name	Surface brightness at 1 GHz ( $\times 10^{-21} \text{ Wm}^{-2}\text{Hz}^{-1}\text{sr}^{-1}$ )	Distance (kpc)	Diameter (pc)	Ref.
1	G4.5+6.8 <sup>b</sup>	Kepler, SN1604, 3C358	318	6.0	5.2	1
2	G11.2-0.3		193	4.4	5.1	2
3	G18.1-0.1		22.9	5.6	9.0	3
4	G18.8+0.3 <sup>b</sup>	Kes 67	26.6	14.0	55.7	4
5	G21.8-0.6	Kes 69	26	5.2	30.3	5
6	G23.3-0.3	W41	14.5	4.2	33.0	6
7	G27.4+0.4	Kes 73, 4C-04.71	56.4	8.65	10.1	6
8	G31.9+0.0 <sup>b</sup>	3C391	103	7.2	12.4	7
9	G33.6+0.1 <sup>b</sup>	Kes 79	33.1	7.0	20.4	8
10	G35.6-0.4		8.2	3.6	13.5	9
11	G41.1-0.3	3C397	294	10.3	10.0	10
12	G43.3-0.2 <sup>b</sup>	W49B	477	10.0	10.1	11
13	G46.8-0.3 <sup>b</sup>	HC30	9.5	7.8	33.7	6
14	G53.6-2.2 <sup>b</sup>	3C400.2, NRAO 611	1.3	2.8	24.8	6

Table 1 – Continued

No.	Catalog name	Other name	Surface brightness ( $\times 10^{-21} \text{ Wm}^{-2} \text{ Hz}^{-1} \text{ sr}^{-1}$ )	Distance (kpc)	Diameter (pc)	Ref.
15	G54.4−0.3 <sup>b</sup>	HC40	2.6	3.3	38.4	12, 2
16	G55.0+0.3		0.25	14.0	70.5	6
17	G65.1+0.6		0.18	9.0	175.6	6
18	G74.0−8.5 <sup>b</sup>	Cygnus Loop	0.86	0.54	30.1	14
19	G78.2+2.1 <sup>b</sup>	$\gamma$ Cygni, DR4	13.4	1.20	20.9	15
20	G84.2−0.8 <sup>b</sup>		5.2	6.0	31.2	16
21	G89.0+4.7 <sup>b</sup>	HB21	3.1	0.8	24.2	6
22	G93.3+6.9	DA 530, 4C(T)55.38.1	2.5	2.2	14.9	37
23	G93.7−0.2	CTB 104A, DA 551	1.5	1.5	34.9	6
24	G94.0+1.0	3C434.1	2.6	3.0	23.9	17
25	G96.0+2.0		0.067	4.0	30.3	6
26	G108.2−0.6		0.32	3.2	57.2	6
27	G109.1−1.0	CTB 109	4.2	3.2	26.1	18
28	G111.7−2.1 <sup>b</sup>	Cassiopeia A, 3C461	16400	3.33	4.84	19
29	G114.3+0.3		0.17	0.7	14.3	6
30	G116.5+1.1 <sup>b</sup>		0.31	1.6	32.2	6
31	G116.9+0.2 <sup>b</sup>	CTB 1	1.04	1.6	15.8	6
32	G119.5+10.2 <sup>b</sup>	CTA 1	0.67	1.4	36.7	6
33	G120.1+1.4 <sup>b</sup>	Tycho, 3C10, SN1572	132	2.5	5.8	20
34	G127.1+0.5	R5	0.89	1.25	16.4	6
35	G132.7+1.3 <sup>b</sup>	HB3	1.06	2.2	51.2	6
36	G152.4−2.1		0.056	1.10	31.1	21
37	G156.2+5.7 <sup>b</sup>		0.062	1.0	32.0	22
38	G160.9+2.6 <sup>b</sup>	HB9	0.98	0.8	30.2	23
39	G166.0+4.3 <sup>b</sup>	VRO 42.05.01	0.55	4.5	57.4	6
40	G180.0−1.7	S147	0.3	0.62	32.5	6
41	G189.1+3.0 <sup>b</sup>	IC443, 3C157	12.2	1.5	19.6	2
42	G190.9−2.2		0.047	1.0	18.8	21
43	G205.5+0.5 <sup>b</sup>	Monoceros Nebula	0.5	1.2	76.8	6
44	G260.4−3.4 <sup>b</sup>	Puppis A, MSH 08-44	6.5	2.2	35.1	6
45	G290.1−0.8	MSH 11-61A	23.8	7.0	33.2	13
46	G292.2−0.5		3.5	8.4	42.3	6
47	G296.5+10.0 <sup>b</sup>	PKS 1209-51/52	1.2	2.1	46.7	24
48	G296.7−0.9		3.8	9.8	31.2	25
49	G296.8−0.3	1156-62	4.8	9.6	46.7	6
50	G308.4−1.4		2.1	9.8	12.0	26, 27
51	G315.4−2.3 <sup>b</sup>	RCW 86, MSH 14-63	4.2	2.3	28.1	6
52	G327.4+0.4	Kes 27	10.2	4.85	29.6	6
53	G327.6+14.6 <sup>b</sup>	SN1006, PKS 1459-41	3.2	1.7	14.8	28
54	G332.4−0.4 <sup>b</sup>	RCW 103	42.1	3.1	9.0	6
55	G337.0−0.1	CTB 33	134	11.0	4.2	6
56	G337.8−0.1	Kes 41	50.2	11.0	23.5	6
57	G338.3−0.0		15.7	11.0	25.6	29
58	G340.6+0.3		20.9	15.0	26.2	6
59	G344.7−0.1		3.8	14.0	40.7	30
60	G346.6−0.2		18.8	7.5	17.4	31
61	G348.5+0.1 <sup>b</sup>	CTB 37A	48.2	9.9	43.2	32
62	G348.7+0.3 <sup>b</sup>	CTB 37B	13.5	13.2	65.3	33

Table 1 – Continued

No.	Catalog name	Other name	Surface brightness ( $\times 10^{-21} \text{ Wm}^{-2} \text{ Hz}^{-1} \text{ sr}^{-1}$ )	Distance (kpc)	Diameter (pc)	Ref.
63	G349.7+0.2 <sup>b</sup>		602	11.5	7.5	34
64	G352.7–0.1		12.5	7.5	15.1	8
65	G359.1–0.5 <sup>b</sup>		3.7	7.6	53.1	35, 36

**Notes.**

<sup>a</sup> Direct distance estimates, inferred from proper motions, shock and radial velocities, HI absorption and polarization, association or interaction with HI, HII and CO molecular clouds, OB associations, pulsars, X-ray observations, optical extinction and low frequency radio absorption.

<sup>b</sup> SNRs from Case and Bhattacharya’s (1998) calibration sample.

**References.** (1) Chiotellis et al. 2012; (2) Case and Bhattacharya 1998; (3) Leahy et al. 2014; (4) Paron et al. 2012; (5) Zhou et al. 2009; (6) Green 2014; Ferrand and Safi-Harb 2012; (7) Su et al. 2014; (8) Giacani et al. 2009; (9) Zhu et al. 2013; (10) Jiang et al. 2010; (11) Zhu et al. 2014; (12) Junkes et al. 1992; (13) Filipović et al. 2005; (14) Blair and Sankrit 2005; (15) Uchiyama et al. 2002; (16) Leahy and Green 2012; (17) Jeong et al. 2013; (18) Kothes and Foster 2012; (19) Alarie et al. 2014; (20) Zhang et al. 2013; (21) Foster et al. 2013; (22) Xu et al. 2007; (23) Leahy and Tian 2007; (24) Giacani et al. 2000; (25) Prinz and Becker 2013; (26) Prinz and Becker 2012; (27) De Horta et al. 2013; (28) Nikolić et al. 2013; (29) Castelletti et al. 2011; (30) Giacani et al. 2011; (31) Yamauchi et al. 2013; (32) Yamauchi et al. 2014; (33) Tian and Leahy 2012; (34) Tian and Leahy 2014; (35) Uchida et al. 1992a; (36) Uchida et al. 1992b; (37) Jiang et al. 2007.

Our main source of information is Green’s updated catalog of Galactic SNRs (2014 May version, Green 2014) and Gilles Ferrand’s database of Galactic SNRs<sup>1</sup> (Ferrand and Safi-Harb 2012). We have additionally searched the literature which provide accurate distances to Galactic shell SNRs that are not included in the above catalogues.

The Galactic sample of calibrators in Paper I contains 60 shell SNRs with direct distance estimates. We have searched the literature to find recent and accurate distances to as many SNRs as available. Here the presented sample contains SNRs with revised distances to 10 objects from the Paper I sample. SNRs with new distance estimates are listed in Table 2.

G309.8+0.0 has been removed from the list of calibrators as we find its distance questionable. Up to now, the main reference was Case and Bhattacharya (1998) who proposed the distance of 3.6 kpc. Actually, these authors cited Huang and Thaddeus (1985) who further mentioned Caswell et al. (1980) as the main reference for this distance. Caswell et al. (1980) only concluded that HI interferometry should permit a distance determination and they proposed to make this measurement when the improvements to the Parkes interferometer are completed.

We have also added the following 6 new SNRs to the original Paper I sample: G18.1–0.1, G35.6–0.4, G152.4–2.1, G190.9–2.2, G296.7–0.9 and G308.4–1.4.

Foster et al. (2013) reported on the discovery of two Galactic SNRs designated G152.4–2.1 and G190.9–2.2, using Canadian Galactic Plane Survey (CGPS) data. They introduce these two extended faint discrete objects discovered in the CGPS and show evidence (mainly through their radio spectral and polarization properties) that classifies them as SNRs. Foster et al. (2013) determined a systemic local standard of rest (LSR) velocities for both SNRs along their lines-of-sight using HI and <sup>12</sup>CO( $J = 1 \rightarrow 0$ ) line data. They obtained distances of  $1.1 \pm 0.1$  kpc and  $1.0 \pm 0.3$  kpc for G152.4–2.1 and G190.9–2.2, respectively.

Two recent studies provided the distance estimate to Galactic SNR G18.1–0.1 and thus we include this remnant among calibrators. Paron et al. (2013) suggested that SNR G18.1–0.1 is located, along the plane of the sky, close to several HII regions (infrared dust bubbles N21 and N22, and the HII regions G018.149–00.283 and G18.197–00.181). They suggest that all of these objects belong to the same complex at a distance of about 4 kpc. However, we adopt 5.6 kpc as the distance to this SNR following the conclusions from more recent paper by Leahy et al. (2014). Later, the authors analysed radio and X-ray observations of G18.1–0.1 and the overlapping and surrounding HII regions. The HI spectrum of SNR G18.1–0.1 shows absorption up to  $100 \text{ km s}^{-1}$  but not beyond, yielding a distance of 5.6 kpc.

<sup>1</sup>A census of high-energy observations of Galactic supernova remnants, Department of Physics and Astronomy at the University of Manitoba, [www.physics.umanitoba.ca/snr/SNRcat](http://www.physics.umanitoba.ca/snr/SNRcat)

**Table 2:** Galactic SNRs with revised distances.

Catalog name	Other name	Paper I (kpc)	Revised distance (kpc)	Method	Reference
G18.8+0.3	Kes 67	12.0	14.0	HI absorption, molecular obser- vations	1
G31.9+0.0	3C391	8.5	7.2	interaction with molecular clouds	2
G84.2-0.8		4.5	6.0	HI absorption	3
G94.0+1.0	3C434.1	5.2	3.0	CO cloud interac- tion	4
G111.7-2.1	Cassiopeia A	3.4	3.33	data from SpI- OMM and Hub- ble <sup>2</sup>	5
G120.1+1.4	Tycho	4.0	2.5	cloud association, HI absorption	6
G327.6+14.6	SN1006	2.2	1.7	shock velocity and proper motion	7
G346.6-0.2		11.0	7.5	X-ray observa- tions	8
G348.5+0.1	CTB 37A	7.9	9.9	X-ray observa- tions	9
G349.7+0.2		18.4	11.5	HI absorption	10

**References.** (1) Paron et al. 2012; Su et al. 2014; (3) Leahy and Green 2012; (4) Jeong et al. 2013; (5) Alarie et al. 2014; (6) Zhang et al. 2013; (7) Nikolić et al. 2013; (8) Yamauchi et al. 2013; (9) Yamauchi et al. 2014; (10) Tian and Leahy 2014.

Prinz and Becker (2013) presented a detailed study of the SNR G296.7–0.9 in the 0.2–12 keV X-ray band, using data from XMM-Newton. Using the deduced spectral parameters from the non-equilibrium ionization (NEI) fit, they derived basic properties of the remnant such as distance  $d$ , post-shock hydrogen density  $n_{\text{H}}$ , swept-up mass  $M$ , remnant age  $t$ , radius in pc  $R_s$ , and shock velocity  $v_s$ . Their analysis indicates the SNR with age between 5800 to 7600 years and a distance of  $9.8^{+1.1}_{-0.7}$  kpc.

The extended radio source in the Galactic plane, G35.6–0.4, was reidentified as a SNR by Green (2009) from radio and infrared survey observations. Zhu et al. (2013) found a plausible distance of  $3.6 \pm 0.4$  kpc using HI,  $^{13}\text{CO}$  emission, and HI absorption spectra. With this distance, the average age of SNR G35.6–0.4 would be about 2300 yr and it implies that SNR G35.6–0.4 is in an early evolutionary stage.

Prinz and Becker (2012) presented a detailed X-ray and radio wavelength study of G308.4–1.4, a candidate SNR in the ROSAT All Sky Survey and the MOST SNR catalog, to identify it as a SNR. The SNR candidate and its central sources were studied using observations from the Chandra X-ray Observatory, Swift, the Australian Telescope Compact

Array (ATCA) at 1.4 and 2.5 GHz and WISE infrared observation at  $24 \mu\text{m}$ . Their analysis revealed that the object is at a distance of  $9.8^{+0.9}_{-0.7}$  kpc and that the progenitor star exploded 5000 to 7500 years ago. Also, De Horta et al. (2013) presented radio-continuum observations of this SNR, made with the ATCA, Molonglo Observatory Synthesis Telescope and the Parkes radio telescope and confirmed that G308.3–1.4 is a SNR with a shell morphology. De Horta et al. (2013) estimate the flux density at 1 GHz to be  $S_{1\text{GHz}} \approx 242$  mJy and we adopt their value.

SNR G43.3–0.2 (W49B) has already been in our previous calibration sample with distance of 10 kpc. Zhu et al. (2014) confirmed this distance using recent radio and infrared data. These authors obtained a kinematic distance of  $\sim 10$  kpc for W49B and suggest that the SNR is likely associated with the CO cloud.

After applying the non-weighted orthogonal regression on the sample containing 65 calibrators from Table 1, we obtained the relation:

$$\Sigma_{1\text{GHz}} = 6.9^{+460}_{-6.8} \cdot 10^{-14} D^{-5.2 \pm 1.3} \text{ Wm}^{-2} \text{ Hz}^{-1} \text{ sr}^{-1}, \quad (2)$$

<sup>2</sup>Authors used the imaging Fourier transform spectrometer Spectromètre Imageur de l’Observatoire du Mont-Mégantic (SpIOMM) to obtain hyperspectral cubes of the Cas A and multi-epoch observations from the Hubble Space Telescope to create a proper motion map, showing the displacement of several filaments over the most part of Cas A.

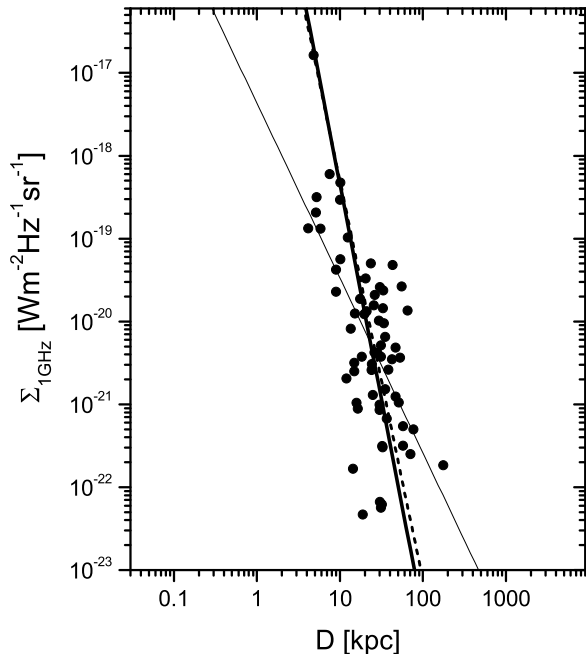


**Fig. 1.** Surface brightness vs. diameter  $\Sigma - D$  relation at 1 GHz for shell SNRs obtained by using the distance calibrators in Table 1. The different methods for minimizing the distance of data from the fitted line are presented. The thin solid line represents the ordinary (vertical) the least squares regression (slope  $\beta = 2.1$ ) while the orthogonal regression is presented by thick line ( $\beta = 5.2$ ). Dashed line represents orthogonal regression obtained in Paper I ( $\beta = 4.8$ ).

where the asymmetric error interval for parameter  $A$  corresponds to  $\Delta \log A = 1.83$  ( $\log A = -13.16$ ). The new relation is slightly steeper than the one obtained in Paper I ( $\beta = 4.8$ ). For shell SNRs calculated distances derived from the updated  $\Sigma - D$  relation are shown in Table 3. In total, 225 Galactic SNRs are shown: 65 SNRs from our calibration sample (just for comparison) and 160 SNRs without available distance estimates.

In order to obtain an accuracy estimate of the obtained  $\Sigma - D$  relation for individual SNR distances, we define fractional errors as:

$$f = \left| \frac{d_I - d_\Sigma}{d_I} \right|, \quad (3)$$

where  $d_I$  is the independently determined distance to an SNR and  $d_\Sigma$  is the distance derived from our relation. Also, this is an indicator of the applicability of our relation for distance determination. The average fractional error for the updated sample is  $\bar{f} = 0.52$  (comparable to  $\bar{f} = 0.47$  in Paper I and  $\bar{f} = 0.41$  obtained by Case and Bhattacharya (1998) for a significantly smaller calibration sample).

## 2.2. $\Sigma - D$ calibration using PDF-based method

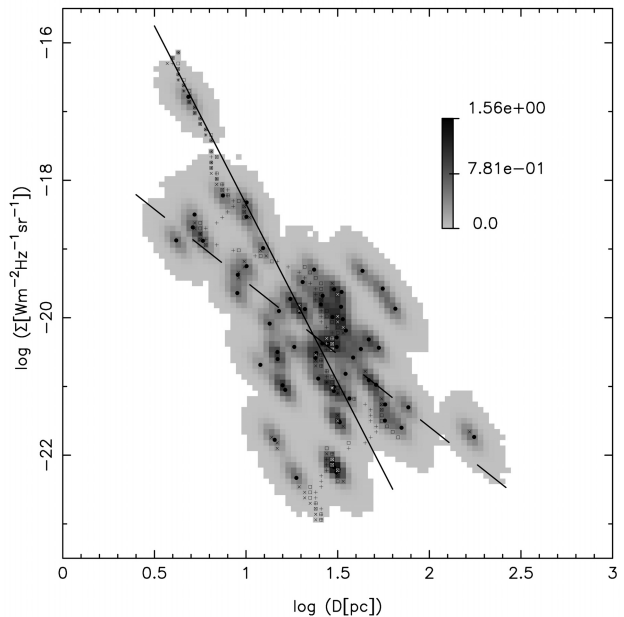


**Fig. 2.** Greyscale reconstructed data PDF. The lattice of  $100 \times 100$  cells is mapped on the variables range shown in the plot. The markers represent parameters of the distributions at fixed  $\Sigma$  values, along the  $D$  axis (rows of the plotted PDF matrix): the mode – diagonal cross, median – open square and mean – cross. The dashed line represents the orthogonal offsets best-fitting line and solid line represents the ordinary least-squares regression.

Calibration of the  $\Sigma - D$  relation can also be done without using neither the orthogonal fitting nor any other standard fitting procedure. Instead, as pointed out by Vukotić *et al.* (2014), random resampling can be used to obtain the probability density function (PDF) of calibration data points in the fitting plane. Therefore, the resulting PDF is used to estimate distance-related properties. Vukotić *et al.* (2014) showed that the PDF-based method for calibration can provide more accurate and more reliable calculations than those obtained by standard linear fitting procedures. Detailed description of algorithm for the calculation of data points density distribution is given in Vukotić *et al.* (2014).

In our analysis,  $10^6$  random resamplings have been done and we mapped resulting samples on the  $10^2 \times 10^2$  lattice spanning the coordinates range shown in Fig. 2. After applying the algorithm from Vukotić *et al.* (2014), the resulting data sample PDF is obtained as a 2D matrix that can be used as the pattern for distance determination (Fig. 2). Thus, this PDF matrix contains more information about the calibration sample than just the line of the best fit. In order to obtain a single value for the distance to a particular SNR, we get a value of the diameter  $D$

from the corresponding PDF distribution of  $D$  at the particular fixed value of  $\log \Sigma$ . This PDF distribution of  $D$  for a fixed value of  $\log \Sigma$  actually represents an 1-dimensional "slice" from a 2-dimensional PDF matrix obtained for the entire data sample.

In Table 3 we present distances to 225 Galactic SNRs inferred from the PDF calibration, in form of three basic statistical properties of these distributions: the median, mode and mean. The median represents the distance corresponding to the diameter  $D$  with equal probability that the value of  $D$  is situated in higher or lower values than median and it changes very slowly with data fluctuations. The mode represents the value which corresponds to the diameter  $D$  having the highest probability and it is representative in cases where this mode peak dominates the entire distribution. The mean distance can be useful in estimating error, although it is more sensitive to fluctuations in data than the median value (Vukotić et al. 2014).

### 2.3. Distances to five newly detected Galactic SNRs

Gerbrandt et al. (2014) presented the results of a systematic search of the Canadian Galactic Plane Survey (CGPS) for faint, extended non-thermal structures that are likely shells of uncatalogued Galactic SNRs. They discovered five new objects which are strong candidates for new SNRs. These five objects are designated by their Galactic coordinate names G108.5+11.0, G128.5+2.6, G149.5+3.2, G150.8+3.8 and G160.1-1.1. CGPS 1420 MHz polarization data and 4.8 GHz polarization data also provide evidence that these objects are newly discovered SNRs.

Gerbrandt et al. (2014) estimated flux densities at 4.8 GHz, 2.7 GHz, 1420 MHz, 408 MHz, and 327 MHz for each object except for G108.5+11.0, for which only three frequency measurements were available: 4.85 GHz, 1420 MHz, and 408 MHz. They also provide flux densities at 1 GHz, deduced by fitting the power-law  $S_\nu \propto \nu^{-\alpha}$  to the frequency spectrum. We then applied our updated empirical Galac-

tic  $\Sigma - D$  relation as well as PDF-based calibration to obtain the diameters and hence distance estimates for these five objects. Flux densities at 1 GHz, angular dimensions and obtained distances are given in Table 3.

We also give the PDF of the diameter variable at the fixed value of  $\log \Sigma$  (respectively -22.3601, -22.3461, -22.4895, -22.0807, -22.0749) for these five very low surface brightness objects (Fig. 3). As noted by Vukotić et al. (2014), in the case when distance estimates for the mode, mean and median are close together, then the mode value should be used as the most probable one. In other cases, where difference is significant, an inspection of PDF may be required, either from a data sample PDF (Fig. 3), or directly from the 2D matrix of PDF presented in form of a graph (Fig. 2). We adopted mode distances for these five new SNRs because all three estimators (the mode, median and mean) were within the range of the highest peak (Fig. 3). As can be seen from Fig. 3, PDF distributions for SNRs G108.5+11.0, G128.5+2.6 and G149.5+3.2 have two dominant peaks of approximately the same probability, so we adopt two distance estimates for them (the last column values in brackets correspond to lower peaks).

The results presented in Table 3 lead to a conclusion that the PDF-based method gives lower diameters than the values estimated from the best fit line (orthogonal fit) and, therefore, gives lower distances for a given angular diameter of the object. The explanation for this can be a denser populated calibrator data point region at  $\log \Sigma \approx -22$  which is situated to the left of the orthogonally fitted line, towards the lower diameters.

These values are obtained using the calibrators from Table 1, however they give a significantly different results than if the orthogonal fitting is used. The average fractional errors (defined by Eq. (3)) for PDF calibration are 0.35, 0.43 and 0.39 for the mode, median and mean distances respectively, and they are notably lower than those in the orthogonal fitting ( $f = 0.52$ ). Thus, the PDF method ensures a greater consistency and more accurate calibrations.

**Table 3:** Distances to five newly discovered candidates for SNRs, along with their integrated flux and spectral properties.

Catalog name	Flux density $S_{1\text{GHz}}$ (mJy)	Angular size (arcmin)	Orthogonal fit distance (kpc)	PDF distance (kpc)			Adopted distance (kpc)
				Mode	Median	Mean	
G108.5+11.0	734	$64.9 \times 39.0$	4.1	2.3	2.2	1.8	2.3 (1.3)
G128.5+2.6	255	$39.6 \times 21.5$	7.0	4.0	3.7	3.0	4.0 (2.3)
G149.5+3.2	590	$55.6 \times 49.3$	4.1	1.3	1.5	1.7	1.3 (2.2)
G150.8+3.8	665	$64.1 \times 18.8$	5.2	2.9	2.9	2.7	2.9
G160.1-1.1	265	$35.9 \times 13.2$	8.3	4.7	4.7	4.3	4.7

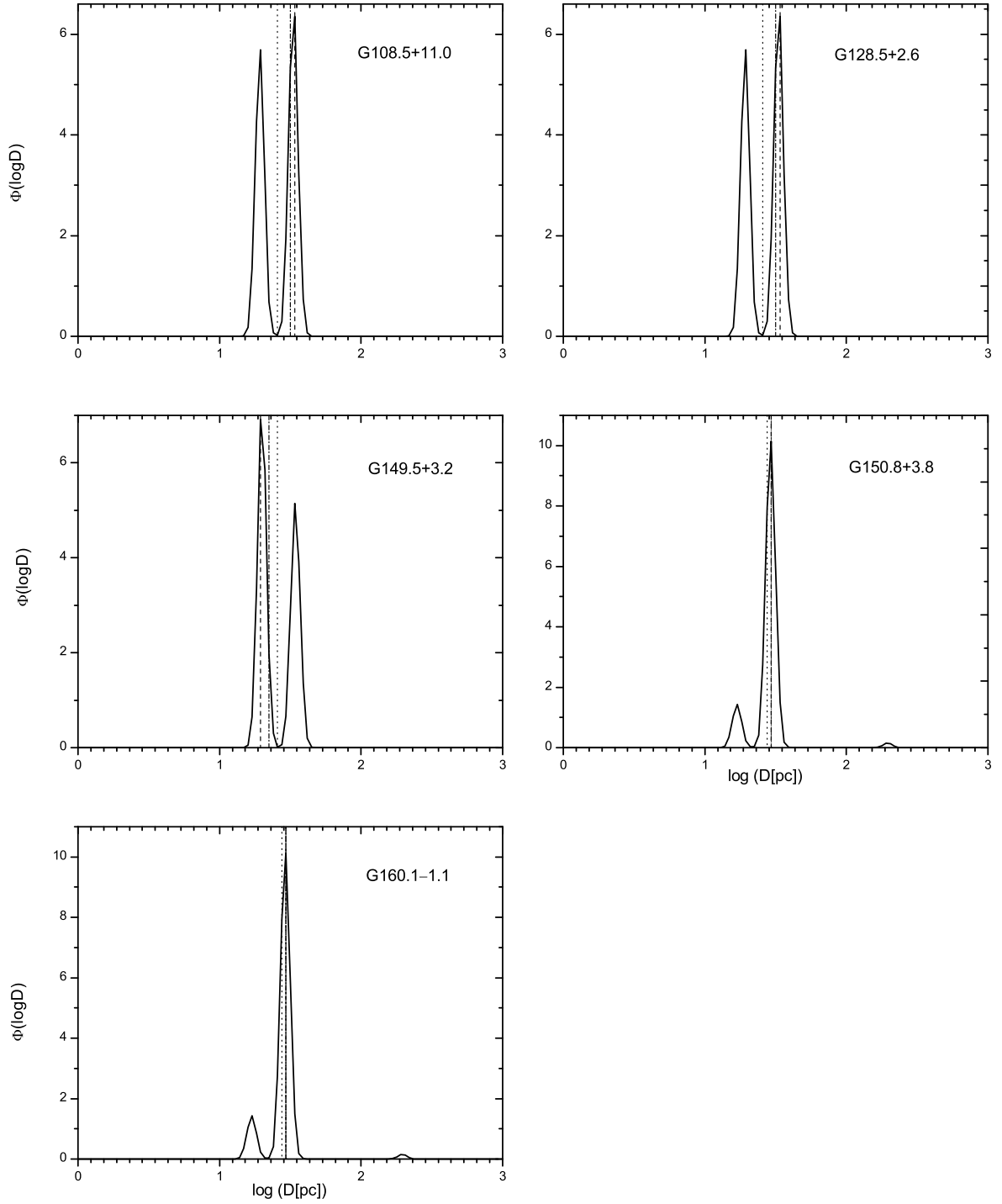


**Fig. 3.** PDF of the diameter variable at the fixed value of  $\log \Sigma$  from the data sample. PDFs are given respectively from G108.5+11.0 (top left) until G160.1-1.1 (bottom left). The first three SNRs have two peaks of similar probability, so we put lower peak values in brackets in the last column of Table 3. Mode, median and mean are presented with dashed, dash-dotted and dotted lines, respectively. The PDF function is such that  $\int_{-\infty}^{+\infty} \Phi(\log D) d(\log D) = 1$  (Vukotić *et al.* 2014).



### 3. DISCUSSION

The  $\Sigma - D$  relation is an important tool in estimating distances to Galactic SNRs in cases where other distance measurements are not applicable. However, we acknowledge its theoretical and statistical inconsistencies. Also, caution is necessary as uncertainties of distance estimates could be higher than 50 % for values obtained using the orthogonal fitting and at least 35 % for PDF-based distance calculation.

The catalog of known Galactic SNRs has grown since our Paper I, from 274 to 294 SNRs. The total number of SNRs with known distances (calibrators) has increased and our Galactic sample now contains 65 shell remnants, which is used to derive a new empirical  $\Sigma - D$  relation. Our improved sample contains revised distances to 10 SNRs from previous sample and we have also added 6 new SNRs to the previous sample. One calibrator is omitted from the previous calibration sample. In addition, we also provide a PDF-based calibration for the updated sample.

Our obtained slope ( $\beta = 5.2$ ) is slightly steeper than this slope in Paper I ( $\beta = 4.8$ ), but it stays within statistical errors. These two  $\Sigma - D$  lines intersect in a point close to  $D \approx 7.9$  pc and  $\Sigma \approx 1.6 \times 10^{-17} \text{ Wm}^{-2}\text{Hz}^{-1}\text{sr}^{-1}$  and therefore the updated relation gives lower distances than those in Paper I for SNRs with surface brightness  $\Sigma < 1.6 \times 10^{-17} \text{ Wm}^{-2}\text{Hz}^{-1}\text{sr}^{-1}$  (almost all Galactic SNRs, an exception among calibrators is Cassiopeia A). This difference increases linearly with decreasing radio surface brightness. Results obtained with updated relation can change the distance scale for Galactic SNRs up to about 15 per cent in comparison with Paper I. The obtained slope is still far from the trivial one ( $\beta = 2.0$ , Urošević 2002, 2003) and it agrees with theoretical predictions for the Sedov phase of the SNR evolution (Sedov subphases should have  $\beta$  slopes from 2 to 5.75, Paper I).

A significant number of selection effects imposes different limitations on statistical studies of Galactic SNRs (e.g. Green 1991, Urošević et al. 2005, 2010). Identification of Galactic SNRs is always accompanied by the difficulty in identifying (1) faint SNRs and (2) small angular size SNRs. The surface-brightness limit affects the completeness of all surveys of Galactic SNRs and the flux densities of many SNRs are poorly determined. Furthermore, Urošević et al. (2010) concluded that the sensitivity selection effect does not have a major impact on the  $\Sigma - D$  slope for the sample of SNRs from starburst galaxy M82. Additionally, the Malmquist bias is present in the Galactic samples, making them incomplete. This is a volume selection effect that favors bright objects because they are sampled from a larger spatial volume in any flux-limited surveys and therefore, it acts against the low surface-brightness remnants. Only an extragalactic set of SNRs does not suffer from the Malmquist bias which is a distance dependent selection effect.

It has been generally accepted that no single  $\Sigma - D$  relation can be constructed for the en-

tire known sample of Galactic SNRs (Arbutina and Urošević 2005). Our current calibration sample contains 65 SNRs in total, which probably have different explosion energies, evolve in different ambient density, and may be in different phases of SNR evolution. Consequently, any single linear  $\Sigma - D$  relation represents only an averaged evolutionary track for Galactic SNRs. Nevertheless, we argue that the orthogonal fitting instead of ordinary least-squares regression (vertical fitting) represents a significant step forward and improves the statistical analysis of the  $\Sigma - D$  relation.

PDF calibration, however, represents another improvement of statistical approach to the  $\Sigma - D$  relation. It is undoubtedly a more reliable method than just a single fitting calibration (orthogonal fitting in our case) as it gets a firmer hold on very important SNRs complex evolutionary features. Also, the importance of local PDF features in statistical distance calibrations that are averaged out in the case of orthogonal fitting should be emphasized. PDF-based statistics is one of the few approaches that can probably deal with different classes of SNRs which is essential for gaining a better understanding of the SNR evolution.

Nevertheless, the orthogonal fitting stays an important method. Having the best fitting line parameters, one can simply calculate the distance to an SNRs without using a specialized bootstrap code which constructs the PDF distribution for a given sample of calibrators. Also, the obtained slope of the empirical  $\Sigma - D$  relation, may have important consequences for the theoretical modeling of SNR evolution.

For a proper  $\Sigma - D$  analysis, the  $L - D$  correlation should also be tested to allow a possible dependence of luminosity on the diameter as  $L_\nu = CD^\delta$ , where  $C$  is constant, following from the luminosity-surface-brightness relation  $L_\nu = \pi^2 D^2 \Sigma_\nu$  (Arbutina et al. 2004). However, our Monte Carlo simulations in Paper I have revealed that the  $L - D$  relation is very sensitive to scatter in the data. Therefore, it is not possible to obtain the  $L - D$  relation for our sample as it is subject to severe scatter and obtained slopes do not have physical meaning.

### 4. SUMMARY

We present a re-analysis of the empirical Galactic  $\Sigma - D$  relation for Galactic SNRs. The empirical  $\Sigma - D$  relation is strongly dependent not only on the regression type due to severe data scatter, but also on the calibration sample containing SNRs with independently determined distances. Following the main conclusion from Paper I that the orthogonal regression is the most accurate slope predictor in data sets with severe scatter, we derive an updated relation by using only the orthogonal regression. We have not analyzed a possible dependence of radio luminosity on the linear diameter ( $L - D$  relation) because this relation is even more sensitive to severe data scatter.

We applied our updated empirical relation to estimate distances to 160 shell-like remnants with unknown distances (Table 5 contains 225 SNRs in

**Table 4:** Distances to 225 shell SNRs calculated from the updated  $\Sigma - D$  relation and PDF-based analysis.

Catalog name	Other name	Flux density (Jy)	Orthogonal fit		PDF distance (kpc)		
			Diameter (pc)	Distance (kpc)	Mode	Median	Mean
G0.0+0.0	Sgr A East	100.0	7.7	9.0	7.5	7.5	7.5
G0.3+0.0		22.0	17.1	5.4	9.3	8.1	7.5
G1.0-0.1		15.0	16.3	7.0	3.9	10.3	9.0
G1.4-0.1		2.0	26.3	9.0	8.2	8.8	8.8
G3.7-0.2		2.3	27.8	7.7	6.6	7.1	7.1
G3.8+0.3		3.0	30.5	5.8	8.5	5.6	5.3
G4.2-3.5		3.2	35.7	4.4	6.7	4.8	4.8
G4.5+6.8 <sup>a</sup>	Kepler, SN1604, 3C358	19.0	10.7	12.3	11.2	11.2	9.1
G4.8+6.2		3.0	30.5	5.8	8.5	5.6	5.3
G5.2-2.6		2.6	31.3	6.0	5.3	5.6	5.3
G5.5+0.3		5.5	24.2	6.2	7.1	7.6	7.6
G5.9+3.1		3.3	31.2	5.4	4.7	5.1	4.7
G6.1+0.5		4.5	26.1	6.1	5.6	6.0	6.0
G6.4+4.0		1.3	44.2	4.9	18.4	7.0	5.7
G6.5-0.4		27.0	20.0	3.8	3.7	5.3	4.9
G7.0-0.1		2.5	29.4	6.7	10.2	6.3	6.3
G7.2+0.2		2.8	26.4	7.6	6.9	7.4	7.4
G7.7-3.7	1814-24	11.0	25.6	4.0	4.6	4.6	4.3
G8.3-0.0		1.2	21.3	16.3	24.3	22.7	19.8
G8.7-5.0		4.4	32.6	4.3	3.9	4.2	3.9
G8.7-0.1	(W30)	80.0	23.0	1.8	2.6	2.4	2.3
G8.9+0.4		9.0	27.6	3.9	3.4	3.7	3.7
G9.7-0.0		3.7	25.7	6.9	7.9	7.9	7.4
G9.8+0.6		3.9	24.8	7.1	8.5	8.5	7.9
G9.9-0.8		6.7	22.3	6.4	9.7	9.1	7.9
G10.5-0.0		0.9	25.2	14.4	16.9	16.9	15.8
G11.0-0.0		1.3	28.5	9.8	8.3	8.9	8.9
G11.1-1.0		5.8	24.8	5.8	6.9	6.9	6.4
G11.1-0.7		1.0	28.6	11.2	9.4	10.1	10.1
G11.1+0.1		2.3	26.5	8.3	7.5	8.1	8.1
G11.2-0.3 <sup>a</sup>		22.0	11.6	10.0	4.5	4.8	5.2
G11.4-0.1		6.0	19.5	8.4	8.4	11.0	11.0
G11.8-0.2		0.7	22.6	19.4	29.1	27.2	25.4
G12.2+0.3		0.8	24.9	15.6	18.5	18.5	17.3
G12.7-0.0		0.8	25.7	14.7	16.9	16.9	15.8
G13.5+0.2		3.5	17.3	13.3	22.7	19.8	18.4
G14.1-0.1		0.5	27.2	17.1	15.1	16.1	16.1
G14.3+0.1		0.6	24.3	18.7	22.7	22.7	21.2
G15.1-1.6		5.5	31.6	4.1	3.5	3.8	3.5
G15.4+0.1		5.6	24.9	5.9	7.0	7.0	6.5
G15.9+0.2		5.0	18.0	10.4	18.4	14.9	13.9
G16.0-0.5		2.7	26.8	7.5	6.7	7.2	7.2
G16.2-2.7		2.5	30.9	6.2	9.0	6.0	5.6
G16.4-0.5		4.6	24.8	6.5	7.8	7.8	7.3
G17.0-0.0		0.5	26.3	18.1	16.5	17.7	17.7
G17.4-2.3		5.0	30.9	4.4	6.4	4.2	3.9
G17.4-0.1		0.4	29.4	16.9	25.6	15.8	15.8

Table 4 – Continued

Catalog name	Other name	Flux density (Jy)	Orthogonal fit		PDF distance (kpc)		
			Diameter (pc)	Distance (kpc)	Mode	Median	Mean
G17.8-2.6		5.0	30.9	4.4	6.4	4.2	3.9
G18.1-0.1 <sup>a</sup>		4.6	20.5	8.8	13.6	11.8	11.0
G18.6-0.2		1.4	23.1	13.2	19.4	18.1	16.9
G18.8+0.3 <sup>a</sup>	Kes 67	33.0	17.3	4.3	7.4	6.5	6.0
G19.1+0.2		10.0	28.3	3.6	3.1	3.3	3.3
G20.4+0.1		9.0	18.0	7.8	13.6	11.0	10.3
G21.0-0.4		1.1	27.0	11.7	10.4	11.1	11.1
G21.5-0.1		0.4	27.4	18.9	16.5	17.7	17.7
G21.6-0.8		1.4	31.1	8.2	7.3	7.8	7.3
G21.8-0.6 <sup>a</sup>	Kes 69	65.0	17.5	3.0	5.1	4.4	4.1
G22.7-0.2		33.0	22.1	2.9	4.5	4.2	3.6
G23.3-0.3 <sup>a</sup>	W41	70.0	19.4	2.5	2.5	3.3	3.3
G24.7-0.6		8.0	23.5	5.4	6.3	6.8	6.8
G25.1-2.3		8.0	37.1	2.6	3.9	3.9	3.1
G27.4+0.0 <sup>a</sup>	4C-04.71	6.0	14.9	12.8	8.4	18.0	14.6
G28.6-0.1		3.0	25.0	8.0	9.4	9.4	8.8
G29.6+0.1		1.5	21.3	14.6	21.7	20.3	17.7
G30.7+1.0		6.0	28.2	4.7	4.0	4.3	4.3
G31.5-0.6		2.0	33.0	6.3	5.6	6.0	5.6
G31.9+0.0 <sup>a</sup>	3C391	25.0	13.2	7.7	3.5	3.5	4.0
G32.0-4.9	3C396.1	22.0	33.0	1.9	1.7	1.8	1.7
G32.4+0.1		0.2	32.2	18.5	16.9	18.1	16.9
G32.8-0.1	Kes 78	11.0	23.2	4.7	6.9	6.4	6.0
G33.2-0.6		3.5	29.6	5.7	8.5	5.3	5.3
G33.6+0.1 <sup>a</sup>	Kes 79, 4C00.70, HC13	20.0	16.9	5.8	10.1	8.8	7.7
G35.6-0.4 <sup>a</sup>		9.0	21.6	5.8	8.5	7.9	6.9
G36.6-0.7		1.0	42.8	5.9	4.7	8.1	7.1
G36.6+2.6		0.7	37.5	8.7	12.7	12.7	11.1
G40.5-0.5		11.0	25.6	4.0	4.6	4.6	4.3
G41.1-0.3 <sup>a</sup>	3C397	25.0	10.6	10.9	10.0	10.0	8.1
G41.5+0.4		1.0	30.0	10.3	15.4	10.1	9.5
G42.0-0.1		0.5	31.5	13.5	11.8	12.7	11.8
G42.8+0.6		3.0	34.1	4.9	4.5	4.9	4.5
G43.3-0.2 <sup>a</sup>	W49B	38.0	9.9	9.8	9.7	9.1	8.4
G43.9+1.6		9.0	39.2	2.2	1.8	3.1	2.7
G45.7-0.4		4.2	30.9	4.8	7.0	4.6	4.3
G46.8-0.3 <sup>a</sup>	(HC30)	17.0	20.3	4.7	4.5	6.4	5.9
G49.2-0.7	(W51)	160.0	17.2	2.0	3.4	2.9	2.7
G53.6-2.2 <sup>a</sup>	3C400.2, NRAO 611	8.0	30.9	3.5	5.1	3.3	3.1
G54.4-0.3 <sup>a</sup>	(HC40)	28.0	27.0	2.3	2.1	2.2	2.2
G55.0+0.3 <sup>a</sup>		0.5	42.4	8.4	6.7	11.7	10.2
G55.7+3.4		1.0	41.4	6.2	5.1	8.8	7.7
G57.2+0.8	(4C21.53)	1.8	28.8	8.2	6.9	7.4	7.4
G59.5+0.1		3.0	28.4	6.5	5.5	5.9	5.9
G64.5+0.9		0.2	39.7	17.1	13.6	23.6	20.6
G65.1+0.6 <sup>a</sup>		5.5	45.0	2.3	0.7	3.5	2.5
G65.3+5.7		42.0	52.3	0.7	0.4	0.4	0.3
G67.7+1.8		1.0	33.6	8.6	8.1	8.7	8.1
G69.7+1.0		2.0	30.7	7.1	10.3	6.8	6.3

Table 4 – Continued

Catalog name	Other name	Flux density (Jy)	Orthogonal fit		PDF distance (kpc)		
			Diameter (pc)	Distance (kpc)	Mode	Median	Mean
G73.9+0.9		9.0	28.8	3.7	3.1	3.3	3.3
G74.0-8.5 <sup>a</sup>	Cygnus Loop	210.0	33.5	0.6	0.6	0.6	0.6
G78.2+2.1 <sup>a</sup>	DR4, gamma Cygni SNR	320.0	19.7	1.1	1.1	1.6	1.5
G82.2+5.3	W63	120.0	26.4	1.2	1.0	1.1	1.1
G83.0-0.3		1.0	27.5	11.9	10.4	11.1	11.1
G84.2-0.8 <sup>a</sup>		11.0	23.7	4.5	5.3	5.7	5.7
G89.0+4.7 <sup>a</sup>	HB21	220.0	26.2	0.9	0.8	0.9	0.9
G93.3+6.9 <sup>a</sup>	DA 530, 4C(T)55.38.1	9.0	27.2	4.0	3.5	3.8	3.8
G93.7-0.2 <sup>a</sup>	CTB 104A, DA 551	65.0	29.9	1.3	1.9	1.2	1.2
G94.0+1.0 <sup>a</sup>	3C434.1	13.0	27.0	3.4	3.0	3.2	3.2
G96.0+2.0 <sup>a</sup>		0.3	53.2	7.0	3.9	3.9	3.6
G108.2-0.6 <sup>a</sup>		8.0	40.5	2.3	1.8	3.1	2.7
G109.1-1.0 <sup>a</sup>	CTB 109	22.0	24.6	3.0	3.6	3.6	3.4
G111.7-2.1 <sup>a</sup>	Cassiopeia A, 3C461	2720.0	5.0	3.4	3.4	3.4	3.4
G114.3+0.3 <sup>a</sup>		5.5	45.9	2.2	0.7	3.3	2.3
G116.5+1.1 <sup>a</sup>		10.0	40.6	2.0	1.6	2.7	2.4
G116.9+0.2 <sup>a</sup>	CTB 1	8.0	32.2	3.3	3.0	3.2	3.0
G119.5+10.2 <sup>a</sup>	CTA 1	36.0	35.1	1.3	2.1	1.5	1.5
G120.1+1.4 <sup>a</sup>	Tycho, 3C10, SN1572	56.0	12.7	5.4	2.4	2.4	2.6
G126.2+1.6		6.0	45.0	2.2	0.7	3.3	2.4
G127.1+0.5 <sup>a</sup>	R5	12.0	33.2	2.5	2.3	2.4	2.3
G132.7+1.3 <sup>a</sup>	HB3	45.0	32.1	1.4	1.2	1.3	1.2
G152.4-2.1 <sup>a</sup>		3.5	56.6	2.0	1.1	1.1	1.0
G156.2+5.7 <sup>a</sup>		5.0	55.5	1.7	1.0	1.0	0.9
G160.9+2.6 <sup>a</sup>	HB9	110.0	32.6	0.9	0.8	0.8	0.8
G166.0+4.3 <sup>a</sup>	VRO 42.05.01	7.0	36.5	2.9	4.3	4.3	3.5
G178.2-4.2		2.0	54.7	2.8	1.5	1.5	1.4
G179.0+2.6		7.0	43.7	2.1	8.2	3.1	2.5
G180.0-1.7 <sup>a</sup>	S147	65.0	40.9	0.8	0.6	1.0	0.9
G182.4+4.3		0.5	63.9	4.4	1.4	1.5	1.6
G189.1+3.0 <sup>a</sup>	IC443, 3C157	164.7	20.0	1.5	1.5	2.1	2.0
G190.9-2.2 <sup>a</sup>		1.3	58.7	3.1	1.7	1.7	1.4
G192.8-1.1	PKS 0607+17	20.0	37.2	1.6	2.4	2.4	2.1
G205.5+0.5 <sup>a</sup>	Monoceros Nebula	140.0	38.1	0.6	0.9	0.9	0.7
G206.9+2.3	PKS 0646+06	6.0	39.2	2.8	2.2	3.9	3.4
G213.0-0.6		21.0	47.4	1.1	0.3	0.8	1.0
G260.4-3.4 <sup>a</sup>	Puppis A, MSH 08-44	130.0	22.6	1.4	2.1	2.0	1.9
G261.9+5.5		10.0	31.1	3.1	2.7	2.9	2.7
G266.2-1.2	RX J0852.0-4622	50.0	36.8	1.1	1.6	1.6	1.3
G272.2-3.2		0.4	41.9	9.6	7.8	13.5	11.8
G279.0+1.1		30.0	37.1	1.3	2.0	2.0	1.7
G284.3-1.8	MSH 10-53	11.0	26.5	3.8	3.4	3.7	3.7
G286.5-1.2		1.4	30.7	8.4	12.3	8.1	7.6
G289.7-0.3		6.2	25.2	5.5	6.4	6.4	6.0
G290.1-0.8 <sup>a</sup>	MSH 11-61A	42.0	17.6	3.7	6.7	5.4	5.1
G292.2-0.5 <sup>a</sup>		7.0	25.5	5.1	5.9	5.9	5.5
G294.1-0.0		2.0	44.8	3.9	1.2	5.8	4.1
G296.1-0.5		8.0	30.9	3.5	5.0	3.3	3.1
G296.5+10.0 <sup>a</sup>	PKS 1209-51/52	48.0	31.2	1.4	1.2	1.3	1.2

Table 4 – Continued

Catalog name	Other name	Flux density (Jy)	Orthogonal fit		PDF distance (kpc)			
			Diameter (pc)	Distance (kpc)	Mode	Median	Mean	
G296.7-0.9 <sup>a</sup>	1156-62	3.0	25.2	7.9	9.3	9.3	8.6	
G296.8-0.3 <sup>a</sup>		9.0	24.0	4.9	5.7	6.1	6.1	
G298.6-0.0		5.0	22.3	7.4	11.2	10.5	9.1	
G299.2-2.9		0.5	39.2	9.6	7.7	13.4	11.7	
G299.6-0.5		1.0	33.2	8.8	7.8	8.4	7.8	
G301.4-1.0	Kes 17	2.1	39.3	4.6	3.7	6.5	5.6	
G302.3+0.7		5.0	27.0	5.5	4.9	5.2	5.2	
G304.6+0.1		14.0	16.6	7.1	12.7	11.0	9.6	
G306.3-0.9		0.2	30.0	25.8	38.4	25.4	23.7	
G308.1-0.7		1.2	32.1	8.5	7.3	7.8	7.3	
G308.4-1.4 <sup>a</sup>		0.2	37.1	15.0	22.3	22.3	18.1	
G309.2-0.6		7.0	23.1	5.9	8.7	8.1	7.6	
G309.8+0.0		17.0	23.5	3.7	4.3	4.7	4.7	
G310.6-0.3		Kes 20B	5.0	20.2	8.7	8.4	11.8	11.0
G310.8-0.4		Kes 20A	6.0	22.8	6.5	9.7	9.1	8.5
G311.5-0.3	RCW 86, MSH 14-63 (MSH 14-57)	3.0	18.6	12.8	17.7	17.7	16.5	
G312.4-0.4		45.0	24.1	2.2	2.5	2.7	2.7	
G312.5-3.0		3.5	30.2	5.5	8.1	5.3	5.0	
G315.4-2.3 <sup>a</sup>		49.0	24.7	2.0	2.4	2.4	2.3	
G315.9-0.0		0.8	39.9	7.3	5.8	10.1	8.8	
G316.3-0.0		20.0	22.1	3.8	5.8	5.4	4.7	
G317.3-0.2		4.7	23.1	7.2	10.6	9.9	9.2	
G318.2+0.1		3.9	38.4	3.5	5.0	5.0	4.4	
G321.9-1.1		3.4	35.3	4.3	6.7	4.8	4.8	
G321.9-0.3		13.0	26.7	3.4	3.1	3.3	3.3	
G323.5+0.1		3.0	26.9	7.1	6.3	6.8	6.8	
G327.2-0.1		0.4	27.4	18.9	16.5	17.7	17.7	
G327.4+0.4 <sup>a</sup>		Kes 27	30.0	20.7	3.4	5.2	4.5	4.2
G327.4+1.0		1.9	30.2	7.4	11.0	7.2	6.8	
G327.6+14.6 <sup>a</sup>		SN1006, PKS 1459-41	19.0	26.0	3.0	3.4	3.4	3.2
G329.7+0.4	Lupus Loop	34.0	25.0	2.4	2.8	2.8	2.6	
G330.0+15.0		350.0	29.6	0.6	0.9	0.5	0.5	
G330.2+1.0		5.0	22.8	7.1	10.6	9.9	9.2	
G332.0+0.2	RCW 103 MSH 16-51, Kes 32	8.0	21.6	6.2	9.1	8.5	7.4	
G332.4-0.4 <sup>a</sup>		28.0	15.8	5.4	3.1	7.7	6.7	
G332.4+0.1		26.0	18.7	4.3	5.9	5.9	5.5	
G332.5-5.6		2.0	42.6	4.2	3.3	5.8	5.0	
G335.2+0.1		16.0	23.4	3.8	4.5	4.8	4.8	
G336.7+0.5	(CTB 33)	6.0	22.7	6.6	9.8	9.2	8.6	
G337.0-0.1 <sup>a</sup>		1.5	13.4	30.6	27.6	20.9	19.5	
G337.2-0.7		1.5	22.8	13.1	19.4	18.1	16.9	
G337.3+1.0	Kes 40	16.0	19.7	5.0	5.0	7.1	6.6	
G337.8-0.1 <sup>a</sup>	Kes 41	18.0	15.3	7.1	4.6	9.8	7.9	
G338.1+0.4		4.0	26.9	6.2	5.5	5.9	5.9	
G338.3-0.0 <sup>a</sup>		6.7	19.1	8.2	8.4	11.0	11.0	
G340.4+0.4		5.0	20.6	8.4	13.0	11.3	10.6	
G340.6+0.3 <sup>a</sup>		5.0	18.1	10.4	18.1	14.7	13.7	
G341.9-0.3		2.5	21.9	10.8	16.6	15.5	13.5	
G342.0-0.2		3.5	23.9	7.9	9.1	9.8	9.8	

Table 4 – Continued

Catalog name	Other name	Flux density (Jy)	Orthogonal fit		PDF distance (kpc)		
			Diameter (pc)	Distance (kpc)	Mode	Median	Mean
G342.1+0.9		0.5	33.6	12.2	11.5	12.3	11.5
G343.1-0.7		7.8	28.2	4.1	3.5	3.7	3.7
G344.7-0.1 <sup>a</sup>		2.5	25.2	8.7	10.1	10.1	9.5
G345.7-0.2		0.6	27.2	15.6	13.7	14.7	14.7
G346.6-0.2 <sup>a</sup>		8.0	18.4	7.9	11.0	11.0	10.3
G347.3-0.5	RX J1713.7-3946	30.0	31.1	1.8	2.6	1.7	1.6
G348.5-0.0		10.0	19.3	6.6	6.7	8.8	8.8
G348.5+0.1 <sup>a</sup>	CTB 37A	72.0	15.4	3.5	2.1	5.1	4.5
G348.7+0.3 <sup>a</sup>	CTB 37B	26.0	19.7	4.0	3.9	5.6	5.2
G349.2-0.1		1.4	25.0	11.7	13.8	13.8	12.9
G349.7+0.2 <sup>a</sup>		20.0	9.5	14.5	11.4	12.2	12.2
G350.0-2.0		26.0	28.6	2.2	1.8	2.0	2.0
G351.7+0.8		10.0	23.0	5.0	7.3	6.8	6.4
G351.9-0.9		1.8	27.2	9.0	7.9	8.5	8.5
G352.7-0.1 <sup>a</sup>		4.0	20.0	9.9	9.7	13.7	12.8
G353.6-0.7		2.5	38.4	4.4	6.3	6.3	5.5
G353.9-2.0		1.0	33.2	8.8	7.8	8.4	7.8
G354.8-0.8		2.8	31.5	5.7	5.0	5.3	5.0
G355.4+0.7		5.0	31.4	4.3	3.8	4.1	3.8
G355.6-0.0		3.0	21.1	10.5	15.7	14.6	12.8
G355.9-2.5		8.0	22.2	5.9	9.0	8.4	7.3
G356.2+4.5		4.0	32.7	4.5	4.1	4.3	4.1
G356.3-1.5		3.0	30.0	6.0	8.9	5.9	5.5
G356.3-0.3		3.0	23.1	9.1	13.3	12.4	11.6
G357.7+0.3		10.0	27.0	3.9	3.4	3.7	3.7
G358.0+3.8		1.5	46.5	4.2	1.3	3.3	4.0
G358.1+0.1		2.0	34.3	5.9	5.4	5.8	5.4
G358.5-0.9		4.0	28.2	5.7	4.9	5.2	5.2
G359.0-0.9		23.0	22.6	3.4	5.1	4.7	4.4
G359.1-0.5 <sup>a</sup>		14.0	25.3	3.6	4.2	4.2	3.9
G359.1+0.9		2.0	27.7	8.3	7.2	7.7	7.7

**Notes.**

<sup>a</sup> SNRs belonging to our updated calibration sample from Table 1. As their distances have been calculated by using the orthogonal fit or PDF-based method, these distances could be significantly different than those in Table 1 which were obtained by using methods mentioned in Paragraph 1.

total, calibrators are also included). We also give distances inferred from the PDF calibration, in the form of three basic statistical properties of these distributions: the median, mode and mean.

We have also applied our relation for estimating distances to five new faint SNRs, discovered with CGPS. PDF-based calculation gives the following results for these SNRs: 2.3 or 1.3 kpc for G108.5+11.0, 4.0 or 2.3 kpc for G128.5+2.6, 1.3 or 2.2 kpc for G149.5+3.2 kpc, 2.9 kpc G150.8+3.8 and 4.7 kpc for G160.1–1.1. Two distance estimates for each of SNRs G108.5+11.0, G128.5+2.6 and G149.5+3.2 have approximately the same probability but never-

theless, we suggest using the mode values 2.3, 4.0 and 1.3 kiloparsecs corresponding to the most dominant peak in PDF distribution. For SNRs G150.8+3.8 and G160.1–1.1 the most probable value (mode) can be used with high confidence.

Although we applied two different methods for distance determination, we expect results obtained by using the PDF-based statistics to be more accurate and more reliable. Nevertheless, PDF-based estimates should also be used with caution (as well as those obtained with the orthogonal fitting) because uncertainties could be as large as about 35-40 % (Vukotić *et al.* 2014).

Taking into account a typical evolution timescale ( $10^5$  yr) of SNRs and an event rate of two supernovae per century in the Galaxy (Dragicevich et al. 1999), 2000 SNRs are expected in our Galaxy. Thus, there are still many "missing" Galactic SNRs, due to difficulties in identifying low surface brightness objects as well as due to the non-conspicuous unresolved "point"-like appearance of very distant SNRs. In the future, high resolution and sensitivity large-scale radio, X-ray and  $\gamma$ -ray surveys of our Galaxy would be crucial in the detection of never-before-seen faint SNRs.

*Acknowledgements* – During the work on this paper, the authors were financially supported by the Ministry of Education and Science of the Republic of Serbia through the Project No. 176005 'Emission nebulae: structure and evolution'. B.V. also acknowledges financial support through the Project No. 176021 'Visible and invisible matter in nearby galaxies: theory and observations'.

## REFERENCES

- Alarie, A., Bilodeau, A. and Drissen, L.: 2014, *Mon. Not. R. Astron. Soc.*, **441**, 2996.
- Arbutina, B., Urošević, D., Stanković, M. and Tešić, Lj.: 2004, *Mon. Not. R. Astron. Soc.*, **350**, 346.
- Arbutina, B. and Urošević, D.: 2005, *Mon. Not. R. Astron. Soc.*, **360**, 76.
- Blair, W. P., Sankrit, R. and Raymond, J. C.: 2005, *Astrophys. J.*, **129**, 2268.
- Case, G. L. and Bhattacharya, D.: 1998, *Astrophys. J.*, **504**, 761.
- Castelletti, G., Giacani, E., Dubner, G., Joshi, B. C., Rao, A. P. and Terrier, R.: 2011, *Astron. Astrophys.*, **536**, 98.
- Caswell, J. L., Haynes, R. F., Milne, D. K. and Wellington, K. J.: 1980, *Mon. Not. R. Astron. Soc.*, **190**, 881.
- Chiotellis, A., Schure, K. M. and Vink, J.: 2012, *Astron. Astrophys.*, **537**, 139.
- De Horta, A. Y., Collier, J. D., Filipović, M. D., Crawford, E. J., Urošević, D., Stootman, F. H. and Tothill, N. F. H.: 2013, *Mon. Not. R. Astron. Soc.*, **428**, 1980.
- Dragicevich, P. M., Blair, D. G. and Burman, R. R.: 1999, *Mon. Not. R. Astron. Soc.*, **302**, 693.
- Ferrand, G. and Safi-Harb, S.: 2012, *Adv. Space Res.*, **49**, 9, 1313.
- Filipović, M. D., Payne, J. L. and Jones, P. A.: 2005, *Serb. Astron. J.*, **170**, 47.
- Foster, T. J., Cooper, B., Reich, W., Kothes, R. and West, J.: 2013, *Astron. Astrophys.*, **549**, A107.
- Gerbrandt, S., Foster, T. J., Kothes, R., Geisbüsch, J. and Tung, A.: 2014, *Astron. Astrophys.*, **566**, A76.
- Giacani, E. B., Dubner, G. M., Green, A. J., Goss, W. M. and Gaensler, B.M.: 2000, *Astron. J.*, **119**, 281.
- Giacani, E., Smith, M. J. S., Dubner, G., Loiseau, N., Castelletti, G. and Paron, S.: 2009, *Astron. Astrophys.*, **507**, 841.
- Giacani, E., Smith, M. J. S., Dubner, G. and Loiseau, N.: 2011, *Astron. Astrophys.*, **531**, 138.
- Green, D. A.: 1984, *Mon. Not. R. Astron. Soc.*, **209**, 449.
- Green, D. A.: 2004, *Bull. Astr. Soc. India*, **32**, 335.
- Green, D. A.: 1991, *Publ. Astron. Soc. Pacific*, **103**, 209.
- Green D. A.: 2014, 'A Catalogue of Galactic Supernova Remnants (2014 May version)', Cavendish Laboratory, Cambridge, United Kingdom (available at "http://www.mrao.cam.ac.uk/surveys/snrs/").
- Huang, Y.-L. and Thaddeus, P.: 1985, *Astrophys. J.*, **295**, L13.
- Jeong, I-G., Koo, B-C., Cho, W.K., Kramer, C., Stutzki, J. and Byun, D-Y.: 2013, *Astrophys. J.*, **770**, 105.
- Jiang, B., Chen, Y., and Wang, Q. D.: 2007, *Astrophys. J.*, **670**, 1142.
- Jiang, B., Chen, Y., Wang, J., Su, Y., Zhou, Xin., Safi-Harb, S. and DeLaney, T.: 2010, *Astrophys. J.*, **712**, 1147.
- Junkes, N., Fuerst, E. and Reich, W.: 1992, *Astron. Astrophys. Suppl. Series*, **96**, 1.
- Kothes, R. and Foster, T.: 2012, *Astrophys. J.*, **746**, L4.
- Leahy, D. A. and Tian, W. W.: 2007, *Astron. Astrophys.*, **461**, 1013.
- Leahy, D. A. and Green, K. S.: 2012, *Astrophys. J.*, **760**, 25.
- Leahy, D., Green K. and Tian, W.: 2014, *Mon. Not. R. Astron. Soc.*, **438**, 1813.
- Nikolić, S., van de Vena, G., Hengb, K., Kupkoc, D., Husemann, B. et al.: 2013, *Science*, **340**, 6128, 45.
- Paron, S., Ortega, M. E., Petriella, A., Rubio, M., Dubner, G. and Giacani, E.: 2012, *Astron. Astrophys.*, **547**, A60.
- Paron, S., Weidmann, W., Ortega, M. E., Albacete Colombo, J. F. and Pichel, A.: 2013, *Mon. Not. R. Astron. Soc.*, **433**, 1619.
- Pavlović, M. Z., Urošević, D., Vukotić, B., Arbutina, B. and Göker, Ü. D.: 2013, *Astrophys. J. Suppl. Series*, **204**, 4. (Paper I).
- Prinz, T. and Becker, W.: 2012, *Astron. Astrophys.*, **544**, A7.
- Prinz, T. and Becker, W.: 2013, *Astron. Astrophys.*, **550**, A33.
- Shklovskii, I. S.: 1960, *Astron. Zh.*, **37**, 256.
- Su, H., Tian, W., Zhu, H. and Xiang, F. Y.: 2014, Proceedings of the International Astronomical Union, IAU Symposium, **296**, 372.
- Tian, W. W. and Leahy, D. A., 2012, *Mon. Not. R. Astron. Soc.*, **421**, 2593.
- Tian, W. W. and Leahy, D. A., 2014, *Astrophys. J.*, **783**, L2.
- Uchida, K., Morris, M. and Yusef-Zadeh, F.: 1992a, *Astron. J.*, **104**, 1533.
- Uchida, K. I., Morris, M., Bally, J., Pound, M. and Yusef-Zadeh, F.: 1992b, *Astrophys. J.*, **398**, 128.
- Uchiyama, Y., Takahashi, T., Aharonian, F. A. and Mattox, J. R.: 2002, *Astrophys. J.*, **571**, 866.
- Urošević, D.: 2002, *Serb. Astron. J.*, **165**, 27.
- Urošević, D.: 2003, *Astrophys. Space Sci.*, **283**, 75.

- Urošević, D., Panmuti, T. G., Duric, N. and Theodorou, A.: 2005, *Astron. Astrophys.*, **435**, 437.
- Urošević, D., Vukotić, B., Arbutina, B. and Sarevska, M.: 2010, *Astrophys. J.*, **719**, 950.
- Vukotić, B., Jurković, M., Urošević, D. and Arbutina, B.: 2014, *Mon. Not. R. Astron. Soc.*, **440**, 2026.
- Xu, J. W., Han, J. L., Sun, X. H., Reich, W., Xiao, L., Reich, P. and Wielebinski, R.: 2007, *Astron. Astrophys.*, **470**, 969.
- Yamauchi, S., Nobukawa, M., Koyama, K. and Yonemori, M.: 2013, *Publ. Astron. Soc. Japan*, **65**, 6.
- Yamauchi, S., Mimani, S., Ota, N. and Koyama, K.: 2014, *Publ. Astron. Soc. Japan*, **66**, 2.
- Zhang, X., Chen, Y., Li, H. and Zhou, X.: 2013, *Mon. Not. R. Astron. Soc.*, **429**, L25.
- Zhou, X., Chen, Y., Su, Y. and Yang, J.: 2009, *Astrophys. J.*, **691**, 516.
- Zhu, H., Tian, W. W., Torres, D. F., Pedalletti, G. and Su, H. Q.: 2013, *Astrophys. J.*, **775**, 95.
- Zhu, H. and Tian, W. W.: 2014, Proceedings of the International Astronomical Union, IAU Symposium, **296**, 378.
- Zhu, H., Tian, W. W. and Zuo, P.: 2014, *Astrophys. J.*, **793**, 95.

## АЖУРИРАНА РЕЛАЦИЈА ИЗМЕЂУ ПОВРШИНСКОГ РАДИО-СЈАЈА И ДИЈАМЕТРА ЗА ГАЛАКТИЧКЕ ОСТАТКЕ СУПЕРНОВИХ

M. Z. Pavlović<sup>1</sup>, A. Dobardžić<sup>1</sup>, B. Vukotić<sup>2</sup> and D. Urošević<sup>1</sup>

<sup>1</sup>*Department of Astronomy, Faculty of Mathematics, University of Belgrade Studentski trg 16, 11000 Belgrade, Serbia*

E-mail: marko@math.rs, aleksandra@math.rs, dejanu@math.rs

<sup>2</sup>*Astronomical Observatory, Volgina 7, 11060 Belgrade 38, Serbia*

E-mail: bvukotic@aob.rs

УДК 524.354–77

Оригинални научни рад

Представљамо ажурирану емпиријску релацију између површинског радио-сјаја и дијаметра ( $\Sigma - D$ ) за остатке супернових у нашој Галаксији. Наш првобитни калибрациони узорак Галактичких остатака са независно одређеним даљинама је поново разматран и допуњен подацима који су публиковани у претходне две године. На калибрациони узорак у  $\log \Sigma - \log D$  скали је примењена метода ортогоналног фитовања као и метода базирана на функцији густине вероватноће. Применом нестандардне ортогоналне регресије постигнута је инваријантност релација  $\Sigma - D$  и  $D - \Sigma$ , у оквиру интервала процене грешке. Наше претходне Монте Карло симулације показале су да би нагиби емпиријских  $\Sigma - D$  релација требало да буду одређивани применом ортогоналне регресије, која се добро показала у примени на узорке са значајним растурањем тачака. Најновији узорак калибратора садржи 65 љускастих остатака. Шест нових остатака супернових је додато у узорак из рада Павловића и сарадника (2013, у даљем тексту Чланак I), један

је изостављен и измењене су даљине за 10 остатака. Нови нагиб је незнатно стрмији ( $\beta \approx 5.2$ ) од нагиба  $\Sigma - D$  релације из Чланка I ( $\beta \approx 4.8$ ). Метода базирана на функцији густине вероватноће користи мапе густине које омогућавају поузданија израчунавања и чувају више информација садржаних у калибрационом узорку. Израчунали смо даљине до пет нових слабих галактичких остатака супернових откривених по први пут од стране Canadian Galactic Plane Survey и добијене су даљине редом 2.3, 4.0, 1.3, 2.9 и 4.7 килопарсека за G108.5+11.0, G128.5+2.6, G149.5+3.2, G150.8+3.8 и G160.1–1.1. Користећи ажурирану емпиријску релацију, одредили смо даљине до љускастих Галактичких остатака и добијени резултати мењају њихову скалу даљина и до 15 процената, у односу на Чланак I. Рачунање из функције густине вероватноће може понекад дати неколико пута веће или мање вредности у поређењу са вредностима добијеним ортогоналним фитом али у просеку ова разлика износи 32, 24 и 18 процената за моду, медијану и средњу вредност даљине.